

# Image-based change detection to reduce false alarms in the Vision1200 synthetic aperture sonar

Dr. C. Erdmann and Dr. J. Groen

ATLAS ELEKTRONIK GmbH  
Sebaldsbrücker Heerstr. 235, 28309 Bremen, Germany  
{carsten.erdmann, johannes.groen}@atlas-elektronik.com

**Abstract** —High-resolution synthetic aperture sonar (SAS) images were processed from a NATO change detection (CD) trial in 2014. An automatic CD processing chain was implemented, consisting of normalization, filtering, coarse registration, fine registration and sub-pixel registration. Various algorithms and parametrizations were used at the different steps in order to determine the best processing chain. Detection quality was determined using Receiver Operating Characteristic (ROC) curves for all combinations. The best CD processing chain was able to reduce the false alarm rate by up to 40 times as compared to conventional detection.

## 1 Introduction

Change detection has recently gained interest in the sonar community. It proves to be highly effective for detecting relevant changes on the sea floor. Data sets collected at different times are scanned for differences which can then be investigated in detail. This potentially reduces the false alarm rate, especially in high-clutter areas, and if done automatically significantly reduces the effort to identify and clear threats in areas that have been previously surveyed.

detection, CCD) and without (incoherent change detection, ICD) use of the phase information.

## 2 Data

Sonar raw data was gathered during a NATO trial in 2014 in the Mediterranean Sea using the high-resolution “Vision MK1 1200” SAS System from ATLAS ELEKTRONIK UK mounted on an ATLAS ELEKTRONIK AUV of the “Sea Otter” class.

Three identical surveys were conducted, using one base survey (no objects) and two surveys with two different sets of 7 mine-like objects (MLO) (see figure 1).

The sea floor showed a strong sand ripple structure, interrupted by few areas with rocks and/or vegetation. MLOs were positioned solely within the ripple area (see figure 2).

The whole data set consisted of 34 images with a total of 116 MLO occurrences.

## 3 Data processing

### 3.1 SAS processing

Raw data were processed using the ATLAS ELEKTRONIK SAS processing chain for high-quality images with a spatial resolution of 2 cm. In addition to the high-quality imagery set, data were reprocessed using incorrect sway settings in order to generate defocused images. For these, a sinusoidal function with the amplitudes of  $0.5\lambda$ ,  $0.75\lambda$  and  $1.5\lambda$  were added to the sway estimation. These artificially defocused images were used to test the robustness of the CD processing chain.

One of the two images of a pair was selected as slave or master. This decision was made based on image quality: the better image was used as the master, the other one slave image.

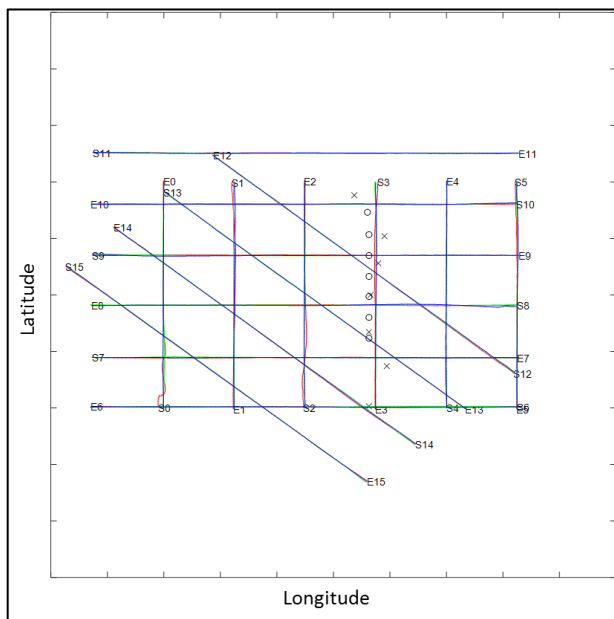


**Fig. 1.** Three identical survey patterns (lines) with 2 sets of MLOs (circles, crosses).  $S_n$  and  $E_n$  denote start and end of track number  $n$ . Axes show latitude and longitude given in decimal degrees.

This study compares various approaches in preprocessing and detection, both with (coherent change

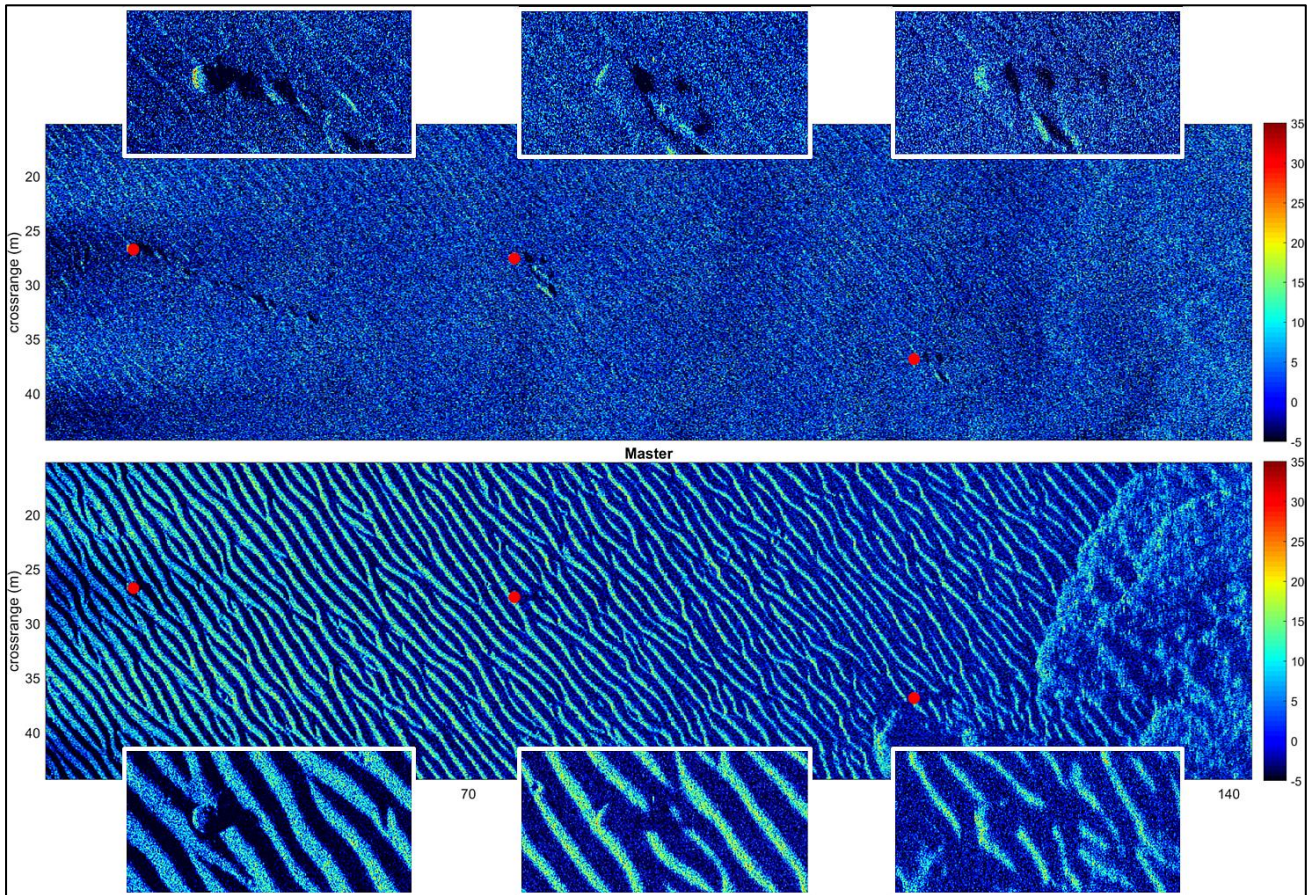


**Fig. 2.** Example of a registration result. Bottom: Master image. Top: difference image after fine registration. Insets show MLO snippets at the red dots. Color bar represents signal intensity

Because errors in crabbing compensation would lead to more serious quality loss than e.g. defocusing, ping-topping correlation was used as a decision parameter. All registration steps were only applied to the slave image; all other steps were applied to both images.

### 3.2 Normalization and filtering

Signal intensity (and signal variance) are range dependent. In order to eliminate this phenomenon two approaches were applied:

- Normalization based on the along-track mean signal intensity or signal variance
- Normalization using a median-based normalization matrix

Effects of AUV roll movements on signal intensity and variance (see shadow areas on the left side in figure 2) could not be eliminated by these global approaches. Therefore an additional normalization matrix was calculated based on the AUV roll sensor data as well as the roll-induced intensity or variance fluctuations.

For CCD, normalization algorithms were applied to complex data instead of intensity in a similar fashion. In this case the amplitude of the complex number was normalized.

Data were used unfiltered or filtered using established filters with speckle-reducing or edge-preserving characteristics:

- Lee-filter: a well-known de-speckle filter with fast processing times [1, 2].
- Anisotropic diffusion filter: a classical edge-preserving filter often used in image processing [3].

### 3.3 Coarse (global) registration

As a first step the slave and master image were registered coarsely. By maximizing the correlation coefficient of the complete images the best crossrange shift, best range shift and best rotation was determined. The rotation resolution was  $0.01^\circ$ , the shift resolution corresponded to the SAS resolution of 2 cm.

This step was performed on intensity data for both ICD and CCD.

### 3.4 Fine registration

Registration, especially fine registration is the crucial step for a successful CD application.

Fine registration of the slave image  $I_S$  to the master image  $I_M$  was performed using cross correlation within a sliding window. Range and cross range displacement  $\Delta x$  and  $\Delta y$  were chosen as the nearest neighbor to the correlation maximum. Due to the small window size rotational effects are negligible, translational corrections are sufficient. This approach results in a 2D morphing field.

For CCD the complex cross correlation was calculated within a sliding window. The subpixel registration precision necessary for good coherence [4, 5] was achieved via cubic interpolation. The algorithm was verified on an image set with only 3 hours of time difference as a proof of concept and showed good correlation.

In order to determine whether the phase information is able to provide further helpful information, phase differences were calculated between master and fine-registered slave image. Although the ripple structure was vaguely visible in the phase image, no enhancements relevant for detection could be found.

Difference images of  $\text{re}(I)$  or  $\text{im}(I)$  were also analyzed, but contrast around MLO positions were identical to those in the intensity difference image, i.e. no significant enhancements could be achieved. Thus, the intensity difference image  $D=20 \log_{10} \left( \frac{I_{\text{MLO}}}{I_{\text{base}}} \right)$  was used for further processing steps, where  $I_{\text{MLO}}$  is the image of interest (i.e. potentially containing MLOs) and  $I_{\text{base}}$  is the base image (i.e. without the change).

### 3.5. Detectors

Detection was performed on the difference images. Since the research described here aims towards the change detection chain, two simple detectors were used instead of the ATLAS ATR processing chain. The first detector is a template matching detector whose template was generated from the mean of all MLO snippets (see figure 3).

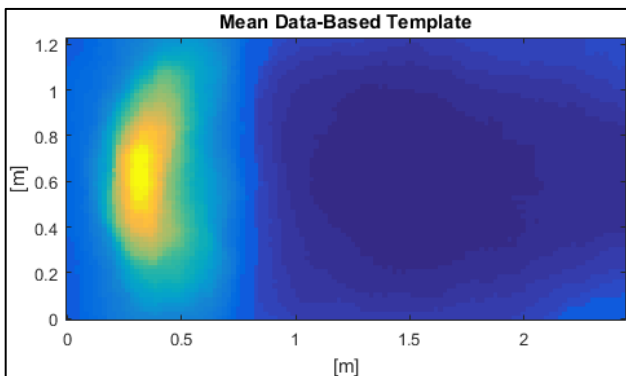


Fig. 3. Template used for the template matching detector

The second detector is based on the signal variance of the difference image, which is locally increased around changes. A constant threshold based on the mean image variance was used.

An essential advantage of using simple detectors is that in this way the SAS images can be transformed to detection maps. Using a simple threshold enables a straightforward analysis via receiver operating characteristics curves. It should be noted however that the absolute detection performance shown here is much lower than that of the ATLAS ATR processing chain.

## 4 Results

### 4.1. Performance

In order to determine the registration quality and thus to be able to compare the different approaches, we defined three criteria:

- Median correlation coefficient  $\rho_{\text{med}}$ : median of the global correlation map.
- Spikiness  $\zeta$ : median of all morphing differences between one estimate and its 4 neighbors on the morphing map.
- Morphing error rate  $\varepsilon$ : fraction of pixels with more than 2 pixels difference to one of its neighbors on the morphing map.

These measures are calculated for all 34 difference images after coherent and incoherent fine registration. For the coherent registration we obtained  $\rho_{\text{med}} = 0.1$ ,  $\zeta = 2.7$  and  $\varepsilon = 60\%$ . In the incoherent case the results are  $\rho_{\text{med}} = 0.25$ ,  $\zeta = 1.1$  and  $\varepsilon = 25\%$ . All three quality criteria are better for the incoherent registration.

For a perfect registration the difference image should be expected to be close to zero in case of no changes. Thus, a further suitable measure is the overall contrast of the difference image. The lower the contrast, the better the registration has performed.

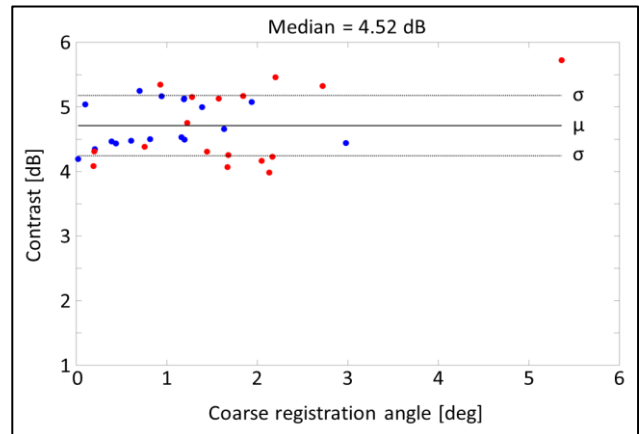


Fig. 4. Image contrast for CCD

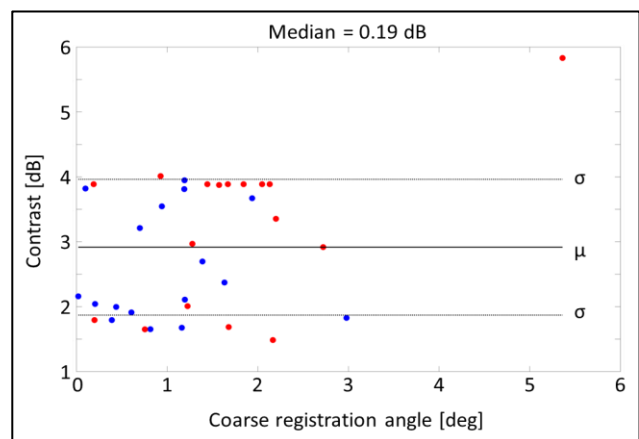
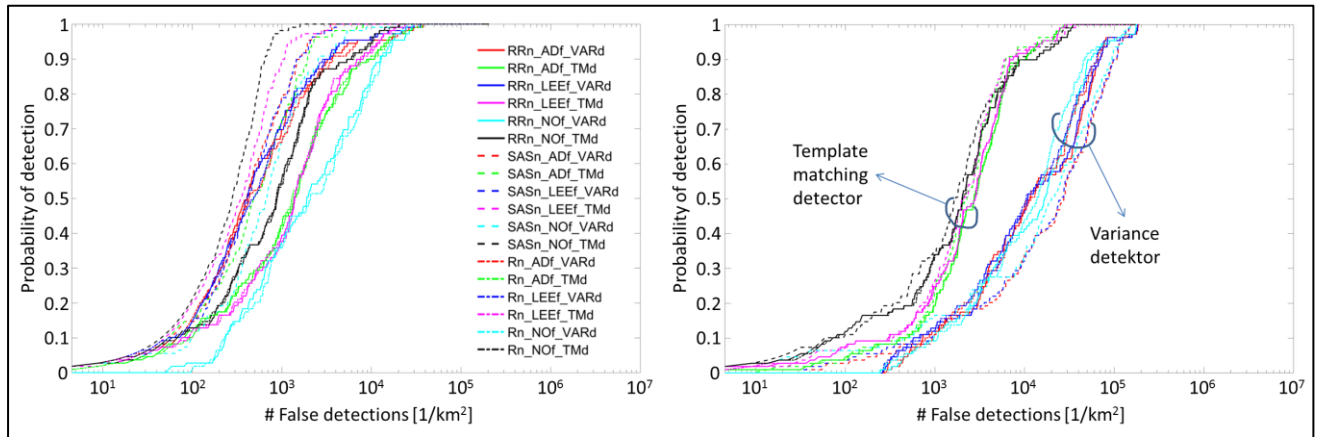


Fig. 5. Image contrast for ICD



**Fig. 6.** ROC curves for all tested combinations. Left: ROC curves after change detection. Right: ROC curves without change detection. Inset legend of left graph explains used methods and holds for both graphs (see text for details). Axes are probability of detection vs. number of false detections per  $\text{km}^2$ .

Figures 4 and 5 show the overall image contrast in the difference image versus the coarse registration angle, which is an indicator whether repeating of the AUV track was successful. We see that the contrast is significantly smaller for ICD (median: 1.9 dB) than for CCD (median: 4.52 dB). Dot color codes for time difference between  $I_{\text{base}}$  and  $I_{\text{MLO}}$  (blue:  $\Delta t = 26$  h, red:  $\Delta t = 56$  h).

## 4.2. Receiver Operating Characteristics

In order to compare the detection performance of the different processing chains, we calculated receiver operating characteristic (ROC) curves for all combinations of normalizations (range, range and roll, median-based), filters (Lee, anisotropic diffusion, no filter) and detectors (template matching, variance threshold). Because defining the probability of false alarm is non-trivial in this dataset, here the number of false alarms per  $\text{km}^2$  is considered.

Figure 6 shows the probability of detection (ordinate) vs. the number of false detections per  $\text{km}^2$ . Line type and color represent different combinations of normalization, filter and detector. The legend codes are combined from the following name parts:

- Normalization code (...n):
  - RRn: roll-range-normalization,
  - SASn: median-based normalization,
  - Rn: range-normalization.
- Filter code (...f):
  - ADf: anisotropic diffusion filter,
  - LEEf: Lee filter,
  - NOf: no filter.
- Detector code (...d):
  - VARd: variance detector
  - TMd: template matching detector

It turns out that the combination of median-based normalization, no filter and the template matching detector result in the best ROC curve, immediately followed by the same combination, based on the Lee-filtered data (SASn\_NOF\_TMd, black dashed line, left plot). The results for the CCD are not shown here, but

were similar, with the same winning combination, all ROC curves were however slightly worse (see table 1).

A change can be observed when the artificially distorted images are analyzed. The combination of median-based normalization and template matching detector shows the best ROC curve for all distortions, but based on the Lee-filtered instead of the unfiltered data (SASn\_LEEf\_TMd). Thus, this combination is the best in terms of detection performance and robustness.

**Table 1.** Comparison of false detections per  $\text{km}^2$  at the specified probability of detection.

	ICD	CCD	ICD 0.5 $\lambda$	ICD 0.75 $\lambda$	ICD 1.5 $\lambda$	No CD
TM 90%	650	720	1,100	1,800	8,700	6,200
TM 95%	780	1,100	1,300	2,400	12,000	14,000
Var 90%	1,600	5,800	2,700	4,200	11,000	47,000
Var 95%	2,000	10,000	3,500	5,600	18,000	76,000

In order to determine the detection gain achieved by using CD, these results can be compared to the ROC curves based on the single data (figure 6, right plot). Obviously the winning combination shows a detection performance that is about 40 times better. Table 1 summarizes the results (number of false alarms per  $\text{km}^2$ ) for both detectors (TM: template matching detector, VAR: variance detector) and a given detection probability (90% and 95%).

Note that detector performance is quite similar in the left plot of figure 6 (set of graphs is homogenous) while it separates into two sets in the right plot. Each of these sets is associated with one detector.

## 5 Discussion

This study tries to determine the most effective CD processing chain for automated use. Based on a sea trial with 3 identical surveys and two sets of MLOs 34 high resolution SAS images with 116 MLO sightings were processed.

Images were normalized and filtered with different approaches. The slave image was then coarse registered to the master image.

For ICD, a morphing map was calculated using the correlation coefficient in a sliding window based on signal intensities. For CCD, a similar approach was used for complex data, using subpixel registration via interpolation. Various approaches were tried to further exploit the phase information in the difference image, but no enhancement could be achieved on the available data.

Registration performance was analyzed using the three criteria correlation coefficient  $\rho_{\text{med}}$ , spikiness  $\xi$  and morphing error  $\varepsilon$ . The incoherent difference images  $D_i$  showed higher  $\rho_{\text{med}}$  and clearly less  $\xi$  and  $\varepsilon$  than the coherent difference images  $D_c$ . Analyzing the image contrast, again  $D_i$  showed significantly smaller contrast values than  $D_c$ .

The smooth background in the difference image (see figure 2, upper image) also shows the successful registration. Both ripples as well as the vegetation area are eliminated, leaving a smooth background with prominent changes. When comparing the associated insets in figure 2, object detection on the master image (bottom) alone would clearly be a challenge.

However, subtracting a ripple image leads to problems in the object shadow area. As shadows are homogenous, subtracting a ripple image leads to interrupted shadows in the difference image (see ripple-associated stripes in upper insets of figure 2). This phenomenon will surely diminish the detection performance of the template matching detector as the template is designed with a homogenous shadow.

As especially the object shadow is a key parameter in object detection, it could be a promising approach to additionally use the shadow information of the original image to further reduce the number of false alarms.

Although the sand ripple structure was macroscopically constant during the 56h trial time period, small changes from biological activity or currents rearranging sand grains are likely to have occurred. Due to the high sensitivity of coherent approaches [6-8] these findings are most likely due to similar effects. This view is supported by the fact that high-correlation coherent images were achieved using image pairs from a different sea trial with a time difference  $\Delta t$  of 3 hours.

All combinations of normalizations, filters and detectors were compared using ROC curves. The best results with respect to false alarm rate and ROC curve steepness are achieved on incoherent difference images  $D_i$  with the median-based normalization and the template matching detector. Although the best curve is gained by using no filter, this is only true for the standard high-quality images, and not for the defocused ones. As soon

as image quality is reduced by defocusing, the Lee-filtered data yield the best results, immediately followed by the anisotropic diffusion filter.

As expected from performance analysis, the coherent fine registration on  $D_c$  images is not able to yield better detection performance. Although the best curves are almost parallel until about 85% detection probability, the coherent curve starts to flatten above that value, resulting in a worse performance. In both cases, however, combinations with the median-based normalization and template matching detector show the best performance.

The robustness analysis with defocused images shows that the combination of the Lee-filter with median-based normalization and template matching detector shows the best results already at slightly defocused images. Thus, this combination would be suggested to be the best CD processing chain.

It should be kept in mind, however, that the CCD results may only hold for the data of this study. There are situations, e.g. with a shorter time span between surveys or more constant environmental parameters, where the coherent approach has benefits and yields better results.

## References

- [1] J.-S. Lee, Digital Image Enhancement and Noise Filtering by Use of Local Statistics. *IEEE Trans. Pattern Anal. Machine Intell.* **2**, 2 (1980)
- [2] J.-S. Lee, Digital Image Smoothing and the Sigma Filter. *Comp. Vis. Graph. Image Proc.* **24** (1983)
- [3] P. Perona, J. Malik, Scale-space and Edge Detection Using Anisotropic Diffusion. *IEEE Trans. Pattern Anal. Machine Intell.* **12**, 7 (1990)
- [4] T. O. Sæbø, R. E. Hansen, H. J. Callow, S. A. V. Synnes, Coregistration of Synthetic Aperture Sonar Images From Repeated Passes. *Proc. Underwater Acoustic Meas. (Kos 2011)*
- [5] I. Quidu, V. Myers, Ø. Midtgaard, R. E. Hansen, Subpixel Image Registration for Coherent Change Detection Between two High Resolution Sonar Passes. *Int. Conf. Underwater Remote Sensing (Brest 2012)*
- [6] A. P. Lyons, D. C. Brown, Temporal Variability of Seafloor Roughness and its Impact on Coherent Change Detection. *Proc. Inst. Acoustics* **32**, 4 (2010)
- [7] A. P. Lyons, D. C. Brown, The Impact of the Temporal Variability of Seafloor Roughness on Synthetic Aperture Sonar Repeat-Pass Interferometry. *IEEE J. Oceanic Eng.* **38**, 1 (2013)
- [8] V. Myers, I. Quidu, T. O. Sæbø, R. Hansen, Results and Analysis of Coherent Change Detection Experiments Using Repeat-Pass Synthetic Aperture Sonar Images. *Underwater Acoustics (Corfu 2013)*

## Acknowledgements

We thank Dr. Holger Schmaljohann (Bundeswehr Technical Center for Ships and Naval Weapons, Maritime Technology and Research, WTD 71) for

valuable discussions and suggestions and Dr. Vince Myers (Defence Research and Development Canada, DRDC) for sharing his expertise on coherent image registration. We also gratefully acknowledge the possibility to use the WTD 71 AUV for the survey and the data for the analysis as well as the Center for Maritime Research and Experimentation, CMRE, for the invitation to conduct this survey.

This study was partially funded by WTD 71.

## Author/Speaker Biographies

**Dr. Carsten Erdmann** studied Neurobiology and Computer Science at the Universities of Konstanz, Tübingen and Freiburg. He received his Ph.D. at the Freie Universität of Berlin on information processing in neurons. In 2008, he joined ATLAS ELEKTRONIK GmbH in Bremen, Germany where he is currently working as a development engineer. His current research interests are image analysis and machine learning with particular focus on MCM operation on SAS images.

**Dr. Johannes Groen** graduated with the M.Sc. degree in mathematics in 1998, from Delft University of Technology in The Netherlands. He has been working as a scientist and a project leader at TNO Defense, Security and Safety in The Hague, The Netherlands. He pursued a Ph.D. at the Seismics and Acoustics group of the Delft University of Technology, which he completed in 2006 with a thesis titled “Adaptive motion compensation in sonar array processing”. He joined the NATO Undersea Research Center’s mine countermeasures department in 2006. Since 2012 he works in the R&D department of the company ATLAS ELEKTRONIK GmbH. His current interest is improvement of the mine hunting systems by migrating science into the products and he is currently involved in the development of the company’s future synthetic aperture sonar suite.